Nanoscale

ROYAL SOCIETY OF CHEMISTRY

PAPER

View Article Online
View Journal | View Issue

Cite this: *Nanoscale*, 2020, **12**, 12831

The alignment-dependent properties and applications of graphene moiré superstructures on the Ru(0001) surface†

Leining Zhang,[a,b] Jichen Dong,[a] Zhaoyong Guan,[a,c] Xiuyun Zhang[a,d] and Feng Ding*[a,b]

The moiré superstructure of graphene on a lattice-mismatched metal substrate has profound effects on the electronic properties of graphene and can be used for many applications. Here, we propose to systematically tune the moiré superstructure of graphene on the Ru(0001) surface by rotating the graphene layer. Our study reveals two kinds of graphene moiré superstructures: (i) the ultra-flat graphene layers with height variations of less than 0.1 Å for rotation angles greater than 20° that have the same structural and electronic properties everywhere, and (ii) the highly corrugated graphene moiré superstructures with height variations from 0.4 to 1.6 Å for rotation angles less than 20°, whose electronic properties are highly modulated by the interaction with the substrate. Moreover, these rotated graphene moiré superstructures can serve as templates to produce matrices of size-tunable metal clusters from a few to ~100 atoms. This study reveals the causes of the structural fluctuation of moiré superstructures of graphene on the transition metal surface and suggests a pathway to tune graphene's electronic properties for various applications.

Received 24th March 2020,
Accepted 12th May 2020

DOI: 10.1039/d0nr02370a

rsc.li/nanoscale

1. Introduction

Since the successful synthesis of graphene *via* the chemical vapor deposition (CVD) approach on Ni and Cu surfaces,[1,2] the growth of graphene CVD on various transition metal (TM) surfaces has been exhaustively explored in the last decade. It is broadly observed that the morphology of the grown graphene is highly dependent on the symmetry, the crystalline lattice constant and the chemical activity of the substrate. Geometrically, a moiré pattern was frequently observed by the superposition of the graphene lattice and the lattice of the metal substrate. On a 4-fold symmetrical substrate, such as Cu (100) or Ni(100) substrate, moiré patterns show either a striped or a rhombic shape depending on the rotation angle between the graphene and substrate.[3–6] On a 3-fold symmetrical surface, such as face-centered cubic (111) or hexagonal close-packed (0001) surface, all moiré patterns show a regular rhombic shape but different periodicities with regard to the rotation angle.[7]

On some active TM surfaces, for example Ru(0001),[8] Rh (111),[9,10] Pb(111),[11] Pt(111)[12,13] and Ir(111)[14,15] substrates, the moiré pattern leads to a corrugated graphene layer with a periodic height variation. Hereafter, we call such a corrugated graphene layer as a graphene moiré superstructure. Many experimental observations revealed that the corrugation of a moiré superstructure is highly dependent on the rotation angle of the graphene lattice with respect to that of the substrate. On the Pt(111) surface, two categories of moiré superstructures were reported: (i) the graphene film has a corrugation of 0.5–0.8 Å at small rotation angles (such as 2°, 3°, and 6°) and (ii) the graphene layer becomes ultra-flat at large rotation angles (14°, 19°, and 30°).[12] In addition, the moiré superstructures of graphene with different rotation angles on the Ir (111) substrate were observed to show that the graphene layer with zero rotation angle has the largest height variation and that the corrugation decays with an increase in the rotation angle.[15]

In comparison with Pt or Ir, Ru has a much stronger interaction with graphene[16–19] and a much larger corrugation of the graphene layer on the Ru(0001) surface has been broadly observed and extensively explored.[20–23] It is worth noting that the thermal expansion difference between graphene and TM

[a]*Centre for Multidimensional Carbon Materials, Institute for Basic Science, Ulsan 44919, Korea. E-mail: f.ding@unist.ac.kr*
[b]*School of Materials Science and Engineering, Ulsan National Institute of Science and Technology, Ulsan 44919, Korea*
[c]*School of Chemistry and Chemical Engineering, Shandong University, Jinan 250100, P. R. China*
[d]*College of Physics Science and Technology, Yangzhou University, Yangzhou 225002, P. R. China*

†Electronic supplementary information (ESI) available. See DOI: 10.1039/d0nr02370a

substrates can also induce corrugations in graphene films, *e.g.*, parallel nanoripple and graphene wrinkles.[24,25] However, compared with other TMs, the very small thermal expansion coefficient of Ru has a very small impact on the corrugation of graphene. Therefore, the Ru(0001) surface is a good substrate for the study of graphene moiré superstructures. Experimentally, graphene generally grows on the Ru(0001) surface with its zigzag direction aligning along the Ru $\langle 2\bar{1}\bar{1}0\rangle$ crystalline direction, forming a moiré superstructure of graphene with a unit cell length of ~2.7 or 3.0 nm and a height oscillation of ~1.8 Å.[26,27] Due to the large corrugation in height, such aligned graphene/Ru(0001) (G/Ru(0001)) superstructures have been used as the most popular templates to synthesize matrices of uniform metal clusters or various organic molecules.[28,29] Generally, Pt, Ru, Ir, Ti, Ni and Rh preferred to be selectively adsorbed at a highly specific site and formed dispersed small clusters, while Pd, Au, Ag, Cu, Co and Fe preferred to form larger clusters crossing different regions.[30–33] Organic molecules, like flat iron phthalocyanine (FePc) and pentacene molecules, were also found to show site preference and orientation preference on the G/Ru(0001) surface.[34,35]

Although graphene shows a preferential orientation on the Ru(0001) substrate during growth, the grown graphene on the Ru(0001) substrate with a very small rotation between the monolayer graphene and substrate has also been observed by few experiments,[27,36,37] and a theoretical study proved that a slight rotation barely affected the geometric and electronic properties of the above-mentioned superstructures of graphene.[38] Besides, very different moiré superstructures of graphene with large rotation angles have been obtained when a graphene layer crosses the grain boundary of the substrate,[39,40] and they can be constructed by graphene transfer.[41–43] To date, a complete theoretical study on the evolution of the rotated graphene moiré superstructure and its properties is yet to be carried out. In this work, by dispersion-corrected density functional theory (DFT) methods, we systematically explored the rotated graphene moiré superstructure on the Ru(0001) surface and studied its potential application in controllable metal cluster synthesis. Depending on the rotation angle, two distinct kinds of graphene layers on the Ru(0001) surface were predicted: (i) the ultra-flat graphene for large rotation angles and (ii) the corrugated graphene, whose properties are highly modulated by the Ru(0001) surface, for small rotation angles. We also showed that the corrugated G/Ru(0001) superstructures can be used as templates to synthesize size-tunable metal clusters from a few to ~100 atoms for various applications.

2. Computational

2.1 Modelling

The primary vectors of graphene film ($\vec{a}$ and $\vec{b}$) and the Ru (0001) substrate ($\vec{c}$ and $\vec{d}$) are shown in Fig. 1(a) and (b). In order to build a common cell of the rotated graphene lattice on a Ru(0001) surface, we considered matching two supercells of graphene and the Ru(0001) surface with limited strain

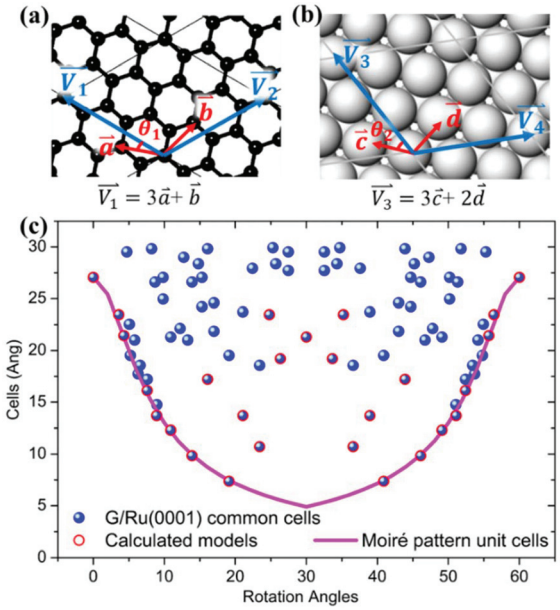

Fig. 1 Schemes of the supercells of graphene (a) and Ru(0001) (b) and the primitive vectors of both. The black and white balls represent the C and Ru atoms, respectively. (c) Some common cells of G/Ru(0001) structures with small cell sizes and limited strain (blue points) and the unit cell size of moiré patterns (curve) *versus* the rotation angle between graphene and the Ru(0001) substrate. The sizes of the calculated G/Ru (0001) structures are marked by red circles.

(<3.0%). To ensure that the shape of both supercells remains a equilateral rhombus with a 120° angle, the vectors of the graphene supercell $(\vec{V}_1, \vec{V}_2)$ and the Ru(0001) supercell $(\vec{V}_3, \vec{V}_4)$ should satisfy

$$\vec{V}_1 = m \cdot \vec{a} + n \cdot \vec{b}, \quad \vec{V}_2 = -n \cdot \vec{a} + (m - n) \cdot \vec{b}. \tag{1}$$

$$\vec{V}_3 = h \cdot \vec{c} + k \cdot \vec{d}, \quad \vec{V}_4 = -k \cdot \vec{c} + (h - k) \cdot \vec{d}. \tag{2}$$

In all our models, the pristine graphene lattice is adopted to avoid the external strain on graphene film, and therefore the sizes of possible common cells of the rotated G/Ru(0001) structures are obtained by considering all combinations of $(\vec{V}_1, \vec{V}_3)$ which satisfy

$$\left|\vec{V}_3\right| \times (1 - 3.0\%) < \left|\vec{V}_1\right| < \left|\vec{V}_3\right| \times (1 + 3.0\%). \tag{3}$$

The searched common cell sizes of G/Ru(0001) superstructures as a function of the rotation angle are denoted by the blue points in Fig. 1(c). Here, the rotation angle between the graphene and the Ru(0001) substrate is calculated by: $\theta = \theta_1 - \theta_2$, where

$$\cos\theta_1 = \frac{m - \frac{1}{2}n}{\sqrt{m^2 + n^2 - mn}}, \quad \cos\theta_2 = \frac{h - \frac{1}{2}k}{\sqrt{h^2 + k^2 - hk}}. \tag{4}$$

Due to the C_{6v} symmetry of graphene and the C_{3v} symmetry of the Ru(0001) surface, the rotation angles can be restricted in a range of [0°, 60°] and a structure with a rotation angle of θ has a symmetrical axis with a rotation angle of 60° − θ.

The reciprocal lattice vector of the G/Ru(0001) moiré pattern can be expressed as the difference of the constituting reciprocal lattice vectors: $\vec{k}_{\text{moirprime e}} = \vec{k}_{\text{G}} - \vec{k}_{\text{Ru}}$.[44] Apparently, two constituting lattices with similar sizes in the reciprocal space result in a larger moiré pattern. In this work, the primitive lattices of graphene and Ru(0001), whose lattice constants are 2.460 Å and 2.706 Å, respectively, are chosen. A lattice mismatch between the graphene and Ru(0001) substrate is defined by the factor[45]

$$\delta = \frac{a_{\text{Ru}} - a_{\text{G}}}{a_{\text{G}}}.$$

The reciprocal lattice vectors of graphene and the Ru(0001) substrate can be expressed as

$$\vec{k}_{\text{G}} = \frac{2\pi}{a_{\text{G}}}(1,0), \quad \vec{k}_{\text{Ru}} = \frac{2\pi}{a_{\text{G}}(1+\delta)}(\cos\varphi, \sin\varphi). \tag{5}$$

Finally, the size of a moiré pattern in real space can be obtained by

$$\lambda = \frac{2\pi}{\left|\vec{k}_{\text{m}}\right|} = \frac{(1-\delta)a_{\text{Gra}}}{\sqrt{2(1-\delta)(1-\cos\varphi)+\delta^2}}, \tag{6}$$

and the size evaluation of the moiré pattern of graphene on the Ru(0001) substrate *versus* the rotation angles is shown in Fig. 1(c).

2.2 Methods

All the calculations are performed within the framework of DFT-D3 method as implemented in the Vienna Ab initio Simulation Package (VASP).[46,47] The exchange–correlation functions are treated by the generalized gradient approximation (GGA),[48] and the interaction between valence electrons and ion cores is carried out by the projected augmented wave (PAW) methods.[49] The energy cutoff for the plane-wave function is set to be 400 eV. The force acting on each atom is set to be less than 0.01 eV Å^{-1}, and an energy convergence of 10^{-4} eV is used as the criterion with regard to structural optimization. For modelling, one-layer graphene on a three-layer Ru(0001) is adopted, and the third layer of the Ru(0001) substrate is fixed. Periodic boundaries are applied in the plane of graphene so that the edge coupling is excluded. In the out-plane direction, the vacuum spacing between neighbouring images is set at least 12 Å to avoid a periodic imaging interaction.

3. Results and discussion

3.1 Structural properties of rotated graphene layers on the Ru (0001) surface

Using the most common G/Ru(0001) superstructure, wherein the graphene zigzag is parallel to the Ru $\langle 2\bar{1}\bar{1}0\rangle$ crystalline direction, as the reference with a rotation angle of zero degree, ten G/Ru(0001) superstructures with a rotation angle interval of ~3° were optimized to explore the rotation-dependent moiré superstructures of graphene.

The atomically optimized moiré superstructures of graphene with different rotation angles are shown in Fig. 2(a). To show the periodic moiré pattern clearly, the coincident spots where the center of a hexagon in the graphene layer is just above a Ru atom are marked by pink Ru atoms. Fig. 2(b) shows the stereo and side views of a few typical structures, from which we can clearly see that the significant graphene height fluctuation at zero degree rotation angle is maintained in graphene with small rotation angles (θ < 20°), while the graphene layers with large rotation angles are all ultra-flat.

A unit cell of the corrugated graphene moiré superstructure is composed of three representative high symmetric sites, namely, ATOP, FCC and HCP, as broadly described in the literature.[50] The difference among the three regions is that the center of a C hexagon corresponds to a Ru atom, an FCC or an HCP site of the ABC-stacked Ru(0001) substrate. The transition regions between two of these three representative sites are called Bridge sites. From the height oscillation, we can see that the distance between the ATOP site and the substrate mostly varies in the range of 2.8–3.7 Å, depending on the rotation angle, which is the typical van der Waals (vdW) distance. A large graphene–substrate distance indicates a weak graphene–Ru(0001) interaction in the ATOP region. In sharp contrast, the distances between all the other sites and the substrate are almost the same, ~2.10 Å, and are rotation angle independent, revealing a strong chemical binding between graphene and the substrate. Geometrically, increasing the rotation angle leads to the formation of a smaller G/Ru(0001) common cell and reduces all the three types of regions in a moiré superstructure. It is found that the highest distance between the graphene layer and the Ru(0001) surface keeps decreasing, while the lowest one remains in the chemical binding range when the moiré superstructure becomes smaller. At 19.10°, the size of the moiré superstructure of graphene becomes only ~7.38 Å with a height fluctuation of ~0.39 Å, and the distance between the ATOP site and the Ru (0001) surface is only ~2.59 Å. Therefore, a sudden change in the graphene layer occurs when the rotation angle becomes greater than 20°. With any rotation angles greater than 20°, the graphene layer becomes ultra-flat and the distance between the graphene layer and the substrate becomes ~3.3 Å everywhere (see Fig. 2(c)).

In a corrugated graphene layer, the C–C bond length is highly site- and orientation-dependent. As has already been demonstrated, in graphene with zero rotation angle, carbon atoms in the ATOP region are sp^2 hybridized and interacted with the substrate *via* the weak vdW interaction.[51] So, the C–C bond lengths in the ATOP region are close to the typical sp^2 C–C bond length or ~1.42 Å.[52] While, in other regions, the carbon atoms interact strongly with the substrate and are slightly prone to sp^3 hybridization, which leads to the elongated C–C bond lengths ranging from 1.45 to 1.46 Å. Our calculations show that all these characteristics in the zero degree moiré superstructure are well maintained in all corrugated graphene layers with a rotation angle of less than 20°, as clearly shown in Fig. 3 and Fig. S1†. In contrast, the C–C bond

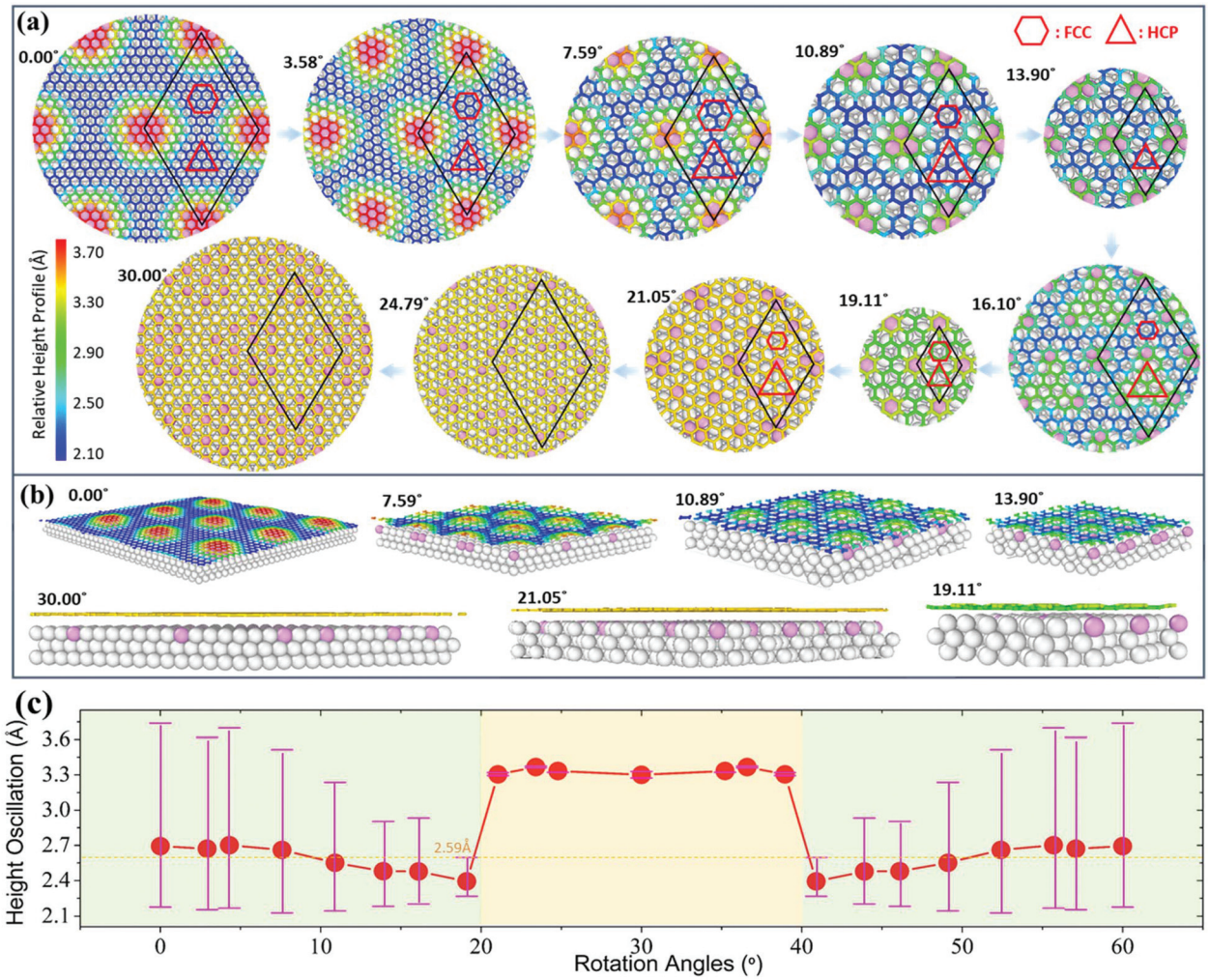

Fig. 2 The structural properties of the rotated graphene on the Ru(0001) surface. (a) The top views of G/Ru(0001) atomic configurations, in which the ATOP regions are marked by pink Ru atoms, FCC and HCP regions are, respectively, marked by hexagons and triangles, and the rhombus represents a unit cell of the G/Ru(0001) superstructure. The height of the graphene layer on the Ru(0001) surface is denoted by a colour profile. (b) The stereo and side views of some typical G/Ru(0001) configurations with different rotation angles. (c) The height oscillation of graphene moiré superstructures, in which the highest, lowest and average distances (points) between graphene and the substrate are shown by error bars.

lengths in the ultra-flat graphene with large rotation angles are highly uniform, ~1.42 Å, and the height fluctuation is less than 0.01 Å. Moreover, it is very clear that the average C–C bond lengths of corrugated graphene moiré superstructures are always larger than that of ultra-flat graphene film. The above analysis of the C–C bond length clearly implies that the corrugated graphene layers on the Ru(0001) surface should have very similar electronic properties to those of zero degree rotation angle graphene moiré superstructures on the Ru (0001) surface, and the electronic properties of ultra-flat graphene layers with large rotation angles are similar everywhere.

3.2 Electronic properties of rotated graphene layers on the Ru(0001) surface

Due to the fact that graphene moiré superstructures mainly show two distinct types of configurations, highly corrugated or ultra-flat, the electronic properties of the moiré superstructures of graphene for one type are generally quite similar, therefore only a few typical G/Ru(0001) superstructures' electronic properties are presented. Many previous studies have demonstrated that the electronic properties of the graphene layer are modulated mainly by the hybridization between the π-orbitals of carbon atoms in graphene and the d orbitals, especially the d_{z_2} orbitals, of the TM substrate.[53,54] In our work, the partial density of states (PDOS) of the rotated graphene layers and the Ru(0001) surface (Fig. 4(a)) are also explored; an obvious overlapping in PDOSs for the HCP and FCC regions of corrugated G/Ru(0001) superstructures implies a strong coupling between the graphene and substrate of these areas. In contrast, the overlapping for ATOP regions of corrugated G/Ru(0001) and all regions of flat G/Ru(0001) is less, indicating a weak coupling of these areas. Such a feature can also be clearly seen in the charge density difference (CDD) plots shown in Fig. 4(b) and (c); charge transfer in the ATOP

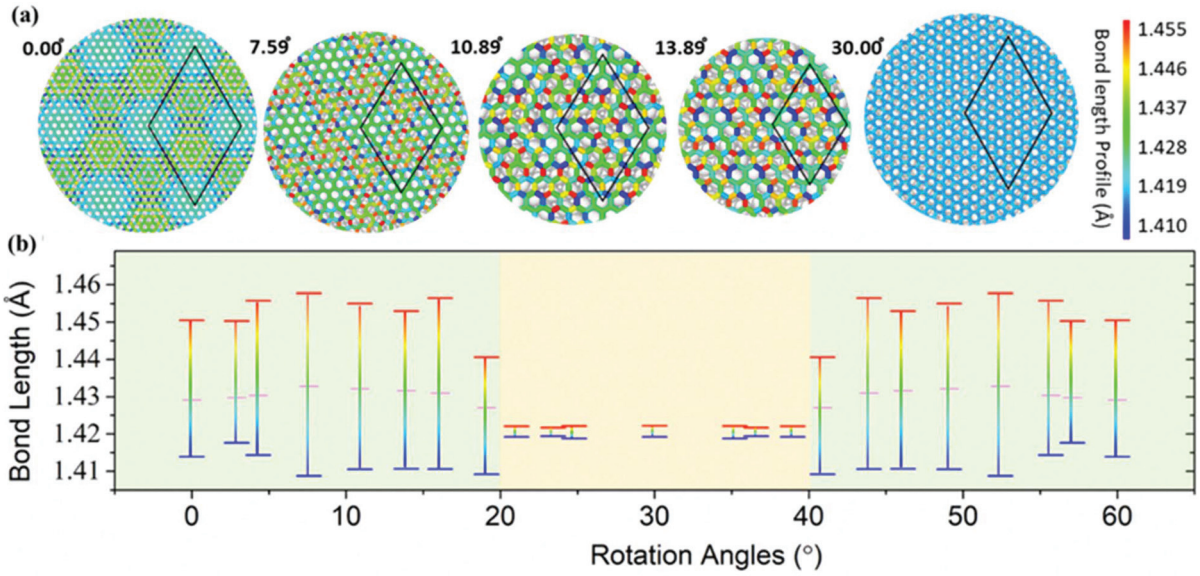

Fig. 3 The C–C bond length profiles of graphene moiré superstructures on the Ru(0001) surface with different rotation angles. (a) The C–C bond length distribution in the rotated graphene on the Ru(0001) surface is marked by colours. (b) The statistics of the C–C bond length distribution as a function of the rotation angle, in which the highest, lowest and average bond lengths are shown by error bars.

region is much smaller than that in other sites, and no charge transfer is seen in the ATOP regions of corrugated G/Ru(0001) superstructures and the whole ultra-flat G/Ru(0001) superstructures with an isosurface level of 0.004 e bohr^{-3}. In sharp contrast, the PDOSs of graphene and the Ru(0001) surface in FCC, HCP and Bridge regions are highly modulated, implying a strong chemical interaction between the graphene layer and the substrate. Further evidence is shown in the CDD plots, where a significant charge transfer from graphene to the Ru (0001) surface can be seen in these three regions. Although above graphene films show ultra-flat configurations, the electronic properties of G/Ru(0001) superstructures with large rotation angles are still modulated by the substrates. Interestingly, it is found that a nearly free-standing graphene film can be obtained by intercalating a layer of oxygen in the interface of a G/Ru(0001) superstructure.[55]

3.3 Using rotated graphene layers on the Ru(0001) surface for the synthesis of tunable Pt clusters

An important application of TM-modulated graphene layer is to be used as the template for the synthesis of uniformed metal clusters. Using the grown graphene on the Ru(0001) surface with zero rotation angle as a template, uniformed metal clusters with a size of up to ~3.0 nm have been synthesized by different approaches.[56–58] A disadvantage of using the G/Ru(0001) superstructure with zero rotation angle is that the sizes of the synthesized clusters are generally very large and hardly tunable. Recalling the above analysis, the graphene layers on the Ru(0001) surface with rotation angles less than 20° maintain the corrugated structure and electronic properties of the zero degree graphene moiré superstructure. So, we propose to use these rotated G/Ru(0001) superstructures as templates to synthesize size-tunable metal clusters.

Because one of the essential conditions for the growth of dispersed metal clusters on the G/Ru(0001) template is that the metal–G/Ru(0001) interaction should be larger than the metal–metal interaction,[33] we firstly compared the adsorption energies of a Pt atom at different regions of G/Ru(0001) superstructures with the Pt–Pt interaction, as shown in Fig. 5(a). The adsorption energy of a Pt atom on the different sites of the G/Ru(0001) superstructure is defined as

$$E_{\mathrm{Ad}} = E_{\mathrm{G/Ru}} + \mu_{\mathrm{Pt}} - E_{\mathrm{Tot}}, \quad (7)$$

where $E_{\mathrm{G/Ru}}$ is the energy of the corresponding G/Ru(0001) superstructure, μ_{Pt} is the chemical potential of a Pt atom in vacuum, and E_{Tot} is the total energy of a Pt atom on the G/Ru (0001) superstructure. The Pt–Pt interaction is estimated by the smallest Pt cluster, *i.e.*, free Pt trimer. For the corrugated G/Ru(0001) superstructures whose rotation angles are less than 19.10°, both HCP and FCC sites always show advantages in templating dispersed metal clusters, while the ATOP site does not when the rotation angles are smaller than ~10°.

Besides, to synthesize the dispersed metal clusters, distinguishing adsorption capacity of different sites of the G/Ru (0001) superstructure is critical. Therefore, the adsorption energies of a Pt atom at different sites are also compared in Fig. 5(a) and the detailed values are shown in Table S1.† On the zero degree G/Ru(0001) superstructure, the differences of the adsorption energies at different sites are quite large. With an increase in the rotation angle, the differences become smaller and smaller until nearly disappear at the 19.10° superstructure. The very small adsorption energy difference at 19.10° means that the preferential nucleation of metal clusters

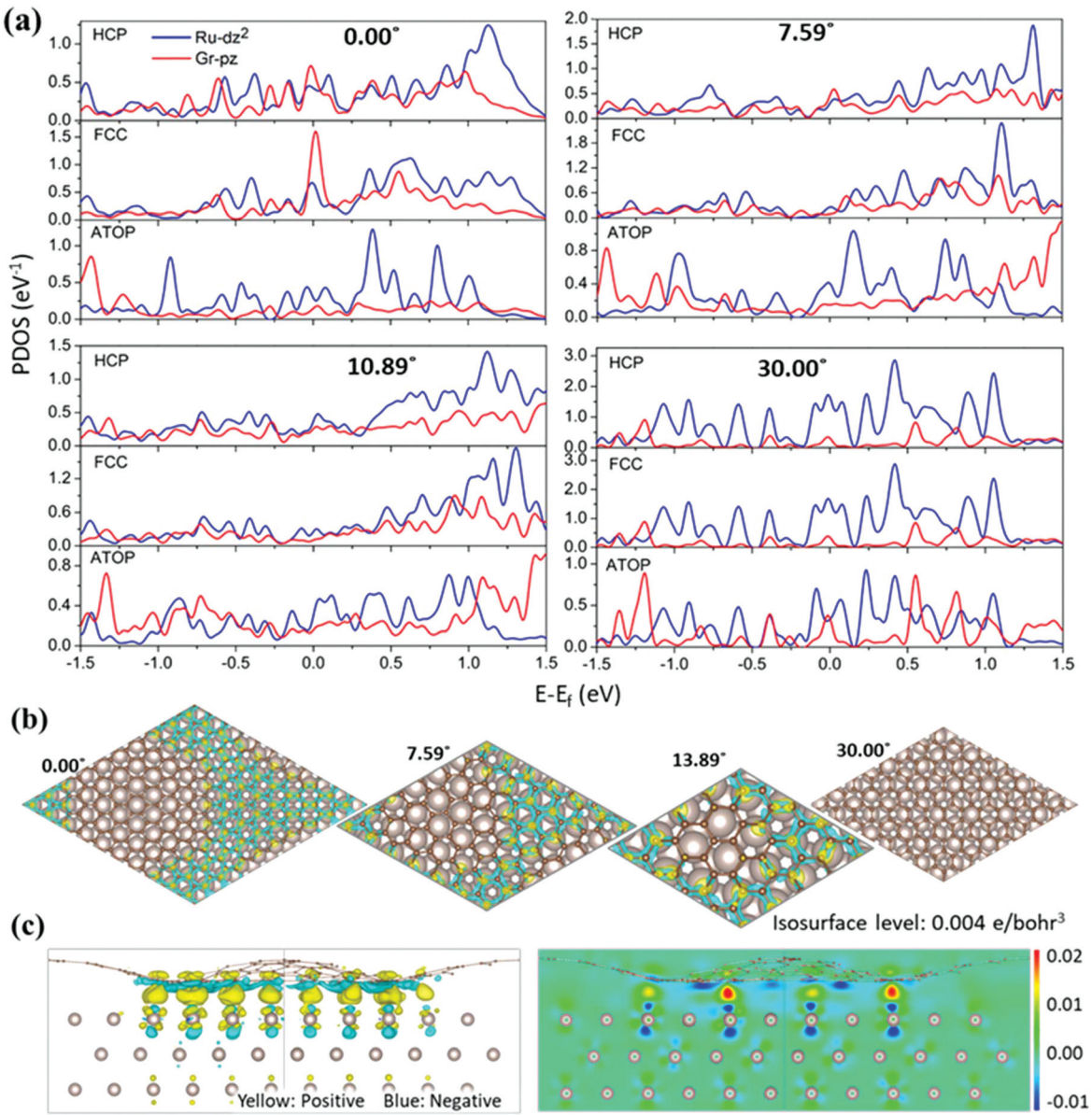

Fig. 4 Electronic properties of different graphene moiré superstructures on the Ru(0001) substrate. (a) The partial density of states (PDOS) of the C and Ru atoms at different sites in the G/Ru(0001) superstructure. (b) Charge density difference (CDD) of G/Ru(0001) with different rotation angles, where the isosurface level of the plot is set as 0.004 e bohr^{-3}. (c) Side view and section of the CDD in the 7.59° G/Ru(0001) superstructure. Yellow and blue colours represent positive and negative charges, respectively.

in a moiré superstructure is not possible, and therefore the 19.10° moiré superstructure cannot serve as a template for the growth of dispersed metal clusters. Similarly, the ultra-flat graphene also cannot serve as a template for the growth of uniformed metal clusters because there is no binding energy difference at different regions.

The atomic configurations of a Pt atom adsorbed at different sites of various moiré superstructures are shown in Fig. 5(b) and Fig. S2.† Overall, C atoms beneath and nearby the adsorbed Pt atom are the mixtures of sp^2 and sp^3 hybridization with a greatly elongated C–C bond length, >1.45 Å. Here, we mark the C atoms bonded to the Pt atom as C_{Pt}. In the zero degree G/Ru(0001) superstructure, both FCC and HCP sites show very high symmetrical characteristics, the three C–C_{Pt} bond lengths are exactly the same and the three carbon neighbours of the C_{Pt} atoms form a strong chemical binding with the Ru atoms beneath them. For the 7.59° G/Ru(0001) superstructure, the feature of the HCP site remains as same as that of the zero degree superstructure, but the Pt atom tends to bond with two C_{Pt} atoms at FCC sites and C–C_{Pt} bonds become shorter than those in the zero degree superstructure, indicating that the degree of sp^3 hybridization of C atoms here becomes weaker and therefore the absorption capacity of a Pt atom weakens. Upon increasing the rotation angle to 13.89°, a

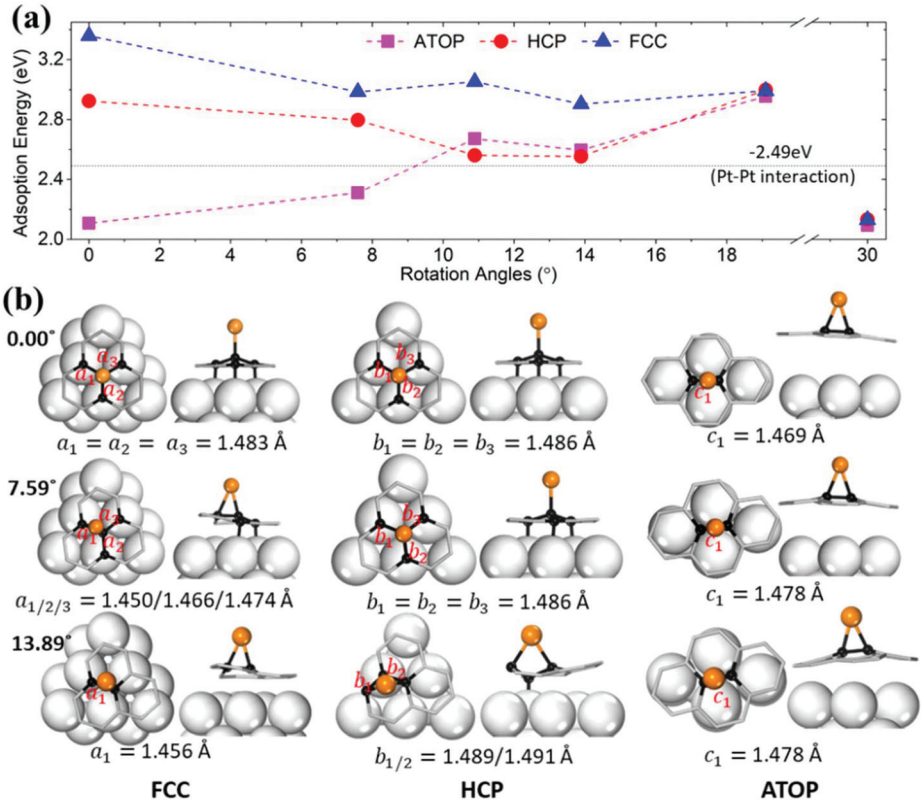

Fig. 5 (a) The adsorption energy of a Pt atom at different sites of G/Ru(0001) superstructures *versus* the rotation angle and Pt–Pt interaction in the Pt trimer. (b) Top and side views of a Pt atom adsorbed on different sites of G/Ru(0001) superstructures, where the C–C bond lengths near the Pt atom are shown.

Pt atom tends to bind with two C_{Pt} atoms at both FCC and HCP sites. However, due to the large rotation, the neighbour C atoms cannot bind with the substrate at the FCC site because there is no Ru atom exactly beneath them, and the shorter C–C bond lengths implied that the degree of sp^3 hybridization of C atoms is further weaken. At the HCP site, the C atom beneath the Pt atom is pushed downwards to bind with a Ru atom of the substrate and the Pt atom forms bonds with its two neighbouring C atoms. At the ATOP site, there are always two C_{Pt} atoms and the C_{Pt}–C_{Pt} bond length becomes larger with an increase in the rotation angle, indicating that the degree of sp^3 hybridization of C atoms at the ATOP site becomes stronger and therefore there is stronger adsorption capacity for the Pt atom. Thus, the absorption capacity for the Pt atom of the special sites is highly related to their sp^3 hybridization degree. In conclusion, although the binding configuration is high rotation angle dependent, the key characteristic that there is a significant binding energy difference between these typical sites remains for the moiré superstructures of graphene with small rotation angles. The above analysis implies that the size-tunable moiré superstructures of graphene with small rotation angles offer possible templates for the synthesis of uniformed metal clusters of different sizes.

In Fig. 6, some large Pt clusters with 1 or 2 layers of atoms templated by the corrugated graphene moiré superstructures on the Ru(0001) surface with different rotation angles are studied. The area of the FCC region of a G/Ru(0001) superstructure is used to determine the size of the Pt clusters because Pt clusters bind to the FCC region more tightly than other regions. On the zero degree G/Ru(0001) template, the sizes of the largest Pt clusters are up to 45 and 45 + 36 = 81 for 1- and 2-layer structures, respectively. With an increase in the rotation angle, the size of Pt clusters decreases, and a cluster comprising only 3 or 4 Pt atoms corresponding to 1- and 2-layer structures can be obtained on the 13.89° G/Ru(0001) template. From the zoom-in sections, one can clearly see that the graphene layer between the Pt cluster and substrate shows distinct sp^3-like features.

To further address the stability of these Pt clusters on the corrugated graphene layers, we calculated the formation energies of Pt clusters on various rotated G/Ru(0001) templates. The formation energy of a Pt cluster on a G/Ru(0001) template is defined as:

$$E_{Pt} = (E_{Tot/Pt} - E_{G/Ru} - N_{Pt} \times \varepsilon_{Pt})/N_{Pt}, \quad (8)$$

where $E_{Tot/Pt}$ is the total energy of Pt clusters on a G/Ru(0001) template, $E_{G/Ru}$ is the energy of the corresponding G/Ru(0001) superstructure, ε_{Pt} is the energy of a Pt atom in the bulk Pt and N_{Pt} is the number of Pt atoms in the corresponding Pt

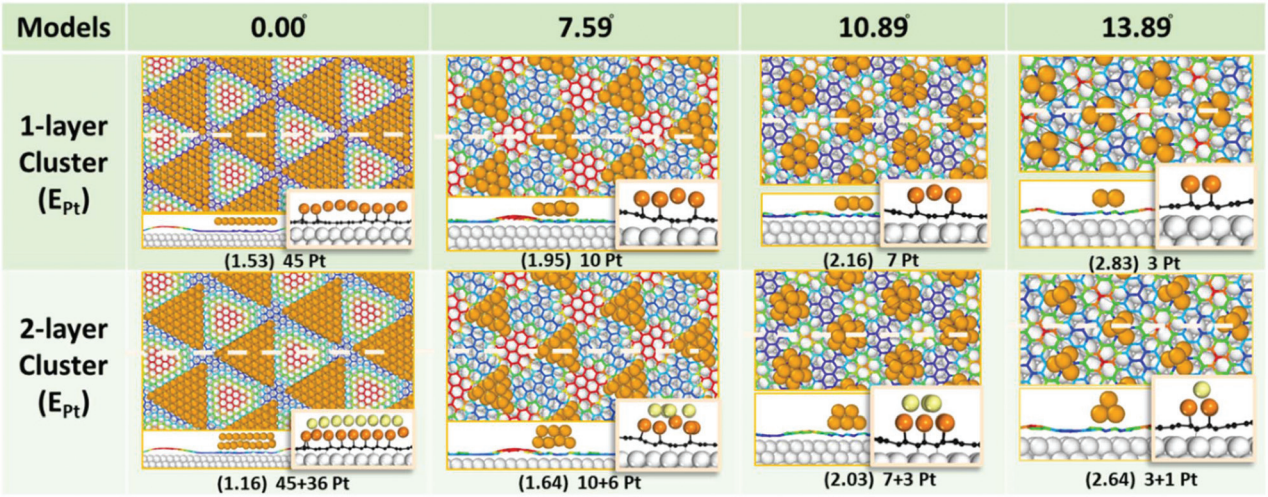

Fig. 6 The top views and sections of the atomic configurations of 1- or 2-layer Pt clusters on different G/Ru(0001) templates. E_{Pt} is the formation energy of Pt clusters on the G/Ru(0001) template in a unit of eV.

cluster. The formation energy of 2-layer Pt clusters is always smaller than that of the corresponding 1-layer structures, implying that 3D Pt clusters on the G/Ru(0001) template are more favoured than 2D clusters. As the rotation angle increases, the formation energies of both 1- and 2-layer clusters increase but their difference becomes less, indicating that G/Ru(0001) templates with small rotation angles prefer multilayer Pt clusters. Besides, it is worth noting that, as proven by a recent work, the Pt clusters templated by such graphene moiré superstructures prefer AA-stacking rather than the conventional ABC-stacking,[59] offering a new route for synthesizing metal clusters with novel structures.

4. Conclusions

Depending on the rotation angle of graphene on the Ru(0001) substrate, two kinds of distinct graphene structures, the ultra-flat graphene films with large rotation angles and the corrugated graphene moiré superstructures with smaller rotation angles, are observed. The ultra-flat graphene film interacts with the substrate by a weak vdW interaction and maintains uniform electronic properties. In contrast, a corrugated graphene moiré superstructure interacts with the substrate through both a weak vdW interaction (near the ATOP site) and a strong chemical binding (near the FCC, HCP and Bridge sites), resulting in highly tuned nonuniform electronic properties. Furthermore, we have shown that the size-tunable graphene moiré superstructures can be used as templates for the formation of size- and structure-tunable metal clusters, varying from ~100 to a few of atoms.

Conflicts of interest

The authors declare no competing financial interest.

Acknowledgements

This work was supported by IBS-R019-D1, NSFC (11574262 and 11904203), and the Fundamental Research Funds of Shandong University (Grant No. 2019GN065). The computational resources from CMCM, IBS are also acknowledged.

Notes and references

1 Q. Yu, J. Lian, S. Siriponglert, H. Li, Y. P. Chen and S.-S. Pei, *Appl. Phys. Lett.*, 2008, **93**, 113103.
2 X. Li, W. Cai, J. An, S. Kim, J. Nah, D. Yang, R. Piner, A. Velamakanni, I. Jung, E. Tutuc, S. K. Banerjee, L. Colombo and R. S. Ruoff, *Science*, 2009, **324**, 1312–1314.
3 H. I. Rasool, E. B. Song, M. Mecklenburg, B. C. Regan, K. L. Wang, B. H. Weiller and J. K. Gimzewski, *J. Am. Chem. Soc.*, 2011, **133**, 12536–12543.
4 J. Cho, L. Gao, J. Tian, H. Cao, W. Wu, Q. Yu, E. N. Yitamben, B. Fisher, J. R. Guest, Y. P. Chen and N. P. Guisinger, *ACS Nano*, 2011, **5**, 3607–3613.
5 Z. Zou, V. Carnevali, M. Jugovac, L. L. Patera, A. Sala, M. Panighel, C. Cepek, G. Soldano, M. M. Mariscal, M. Peressi, G. Comelli and C. Africh, *Carbon*, 2018, **130**, 441–447.
6 Y. Murata, V. Petrova, B. B. Kappes, A. Ebnonnasir, I. Petrov, Y.-H. Xie, C. V. Ciobanu and S. Kodambaka, *ACS Nano*, 2010, **4**, 6509–6514.
7 Y. Dedkov, E. Voloshina and M. Fonin, *Phys. Status Solidi B*, 2015, **252**, 451–468.
8 Y. Pan, H. Zhang, D. Shi, J. Sun, S. Du, F. Liu and H.-j. Gao, *Adv. Mater.*, 2009, **21**, 2777–2780.
9 P. Stojanov, E. Voloshina, Y. Dedkov, S. Schmitt, T. Haenke and A. Thissen, *Procedia Eng.*, 2014, **93**, 8–16.
10 E. N. Voloshina, Y. S. Dedkov, S. Torbrügge, A. Thissen and M. Fonin, *Appl. Phys. Lett.*, 2012, **100**, 241606.

11 S.-Y. Kwon, C. V. Ciobanu, V. Petrova, V. B. Shenoy, J. Bareño, V. Gambin, I. Petrov and S. Kodambaka, *Nano Lett.*, 2009, **9**, 3985–3990.
12 M. Gao, Y. Pan, L. Huang, H. Hu, L. Z. Zhang, H. M. Guo, S. X. Du and H. J. Gao, *Appl. Phys. Lett.*, 2011, **98**, 033101.
13 P. Merino, M. Švec, A. L. Pinardi, G. Otero and J. A. Martín-Gago, *ACS Nano*, 2011, **5**, 5627–5634.
14 J. Coraux, A. T. N'Diaye, C. Busse and T. Michely, *Nano Lett.*, 2008, **8**, 565–570.
15 L. Meng, R. Wu, L. Zhang, L. Li, S. Du, Y. Wang and H. J. Gao, *J. Phys.: Condens. Matter*, 2012, **24**, 314214.
16 Q. Yuan, B. I. Yakobson and F. Ding, *J. Phys. Chem. Lett.*, 2014, **5**, 3093–3099.
17 X. Zhang, Z. Xu, L. Hui, J. Xin and F. Ding, *J. Phys. Chem. Lett.*, 2012, **3**, 2822–2827.
18 J. Dong, L. Zhang, K. Zhang and F. Ding, *Nanoscale*, 2018, **10**, 6878–6883.
19 P. W. Sutter, J. I. Flege and E. A. Sutter, *Nat. Mater.*, 2008, **7**, 406–411.
20 B. Wang, M. L. Bocquet, S. Marchini, S. Gunther and J. Wintterlin, *Phys. Chem. Chem. Phys.*, 2008, **10**, 3530–3534.
21 K. Donner and P. Jakob, *J. Chem. Phys.*, 2009, **131**, 164701.
22 C. C. Silva, M. Iannuzzi, D. A. Duncan, P. T. P. Ryan, K. T. Clarke, J. T. Küchle, J. Cai, W. Jolie, C. Schlueter, T.-L. Lee and C. Busse, *J. Phys. Chem. C*, 2018, **122**, 18554–18561.
23 E. Voloshina and Y. Dedkov, *Phys. Rev. B*, 2016, **93**, 235418.
24 P. R. Shaina, L. George, V. Yadav and M. Jaiswal, *J. Phys.: Condens. Matter*, 2016, **28**, 085301.
25 L. Meng, Y. Su, D. Geng, G. Yu, Y. Liu, R.-F. Dou, J.-C. Nie and L. He, *Appl. Phys. Lett.*, 2013, **103**, 251610.
26 D.-E. Jiang, M.-H. Du and S. Dai, *J. Chem. Phys.*, 2009, **130**, 074705.
27 S. Marchini, S. Günther and J. Wintterlin, *Phys. Rev. B: Condens. Matter Mater. Phys.*, 2007, **76**, 075429.
28 M. Sicot, P. Leicht, A. Zusan, S. Bouvron, O. Zander, M. Weser, Y. S. Dedkov, K. Horn and M. Fonin, *ACS Nano*, 2012, **6**, 151–158.
29 A. T. N'Diaye, S. Bleikamp, P. J. Feibelman and T. Michely, *Phys. Rev. Lett.*, 2006, **97**, 215501.
30 Z. Zhou, F. Gao and D. W. Goodman, *Surf. Sci.*, 2010, **604**, L31–L38.
31 B. Wang, B. Yoon, M. Konig, Y. Fukamori, F. Esch, U. Heiz and U. Landman, *Nano Lett.*, 2012, **12**, 5907–5912.
32 E. Sutter, P. Albrecht, B. Wang, M.-L. Bocquet, L. Wu, Y. Zhu and P. Sutter, *Surf. Sci.*, 2011, **605**, 1676–1684.
33 B. Wang and M.-L. Bocquet, *J. Phys. Chem. Lett.*, 2011, **2**, 2341–2345.
34 G. Li, L. Huang, W. Xu, Y. Que, Y. Zhang, J. Lu, S. Du, Y. Liu and H. J. Gao, *Philos. Trans. R. Soc., A*, 2014, **372**, 20130015.
35 H. G. Zhang, J. T. Sun, T. Low, L. Z. Zhang, Y. Pan, Q. Liu, J. H. Mao, H. T. Zhou, H. M. Guo, S. X. Du, F. Guinea and H. J. Gao, *Phys. Rev. B: Condens. Matter Mater. Phys.*, 2011, **84**, 245436.
36 K. L. Man and M. S. Altman, *Phys. Rev. B: Condens. Matter Mater. Phys.*, 2011, **84**, 235415.
37 B. Borca, S. Barja, M. Garnica, M. Minniti, A. Politano, J. M. Rodriguez-García, J. J. Hinarejos, D. Farías, A. L. V. d. Parga and R. Miranda, *New J. Phys.*, 2010, **12**, 093018.
38 B. Wang and M. L. Bocquet, *Nanoscale*, 2012, **4**, 4687–4693.
39 E. Sutter, P. Albrecht and P. Sutter, *Appl. Phys. Lett.*, 2009, **95**, 133109.
40 E. Sutter, B. Wang, P. Albrecht, J. Lahiri, M. L. Bocquet and P. Sutter, *J. Phys.: Condens. Matter*, 2012, **24**, 314201.
41 W. S. Leong, H. Wang, J. Yeo, F. J. Martin-Martinez, A. Zubair, P.-C. Shen, Y. Mao, T. Palacios, M. J. Buehler, J.-Y. Hong and J. Kong, *Nat. Commun.*, 2019, **10**, 867.
42 J. W. Suk, A. Kitt, C. W. Magnuson, Y. Hao, S. Ahmed, J. An, A. K. Swan, B. B. Goldberg and R. S. Ruoff, *ACS Nano*, 2011, **5**, 6916–6924.
43 J. Kang, D. Shin, S. Bae and B. H. Hong, *Nanoscale*, 2012, **4**, 5527–5537.
44 A. T. N'Diaye, J. Coraux, T. N. Plasa, C. Busse and T. Michely, *New J. Phys.*, 2008, **10**, 043033.
45 S. Tang, H. Wang, Y. Zhang, A. Li, H. Xie, X. Liu, L. Liu, T. Li, F. Huang, X. Xie and M. Jiang, *Sci. Rep.*, 2013, **3**, 2666.
46 G. Kresse and J. Furthmüller, *Comput. Mater. Sci.*, 1996, **6**, 15–50.
47 G. Kresse and J. Hafner, *Phys. Rev. B: Condens. Matter Mater. Phys.*, 1993, **48**, 13115–13118.
48 J. P. Perdew, K. Burke and M. Ernzerhof, *Phys. Rev. Lett.*, 1996, **77**, 3865–3868.
49 G. Kresse and D. Joubert, *Phys. Rev. B: Condens. Matter Mater. Phys.*, 1999, **59**, 1758–1775.
50 E. Voloshina and Y. Dedkov, *Phys. Chem. Chem. Phys.*, 2012, **14**, 13502–13514.
51 L. Zhu and F. Ding, *Nanoscale Horiz.*, 2019, **4**, 625–633.
52 L. Pauling, *J. Chem. Educ.*, 1992, **69**, 519.
53 A. L. Hsu, R. J. Koch, M. T. Ong, W. Fang, M. Hofmann, K. K. Kim, T. Seyller, M. S. Dresselhaus, E. J. Reed, J. Kong and T. Palacios, *ACS Nano*, 2014, **8**, 7704–7713.
54 P. A. Khomyakov, G. Giovannetti, P. C. Rusu, G. Brocks, J. van den Brink and P. J. Kelly, *Phys. Rev. B: Condens. Matter Mater. Phys.*, 2009, **79**, 195425.
55 E. Voloshina, N. Berdunov and Y. Dedkov, *Sci. Rep.*, 2016, **6**, 20285.
56 J. Díez-Albar, M. D. Jiménez-Sánchez and J. M. Gómez-Rodríguez, *J. Phys. Chem. C*, 2019, **123**, 5525–5530.
57 Y. Pan, H. Zhang, D. Shi, J. Sun, S. Du, F. Liu and H.-j. Gao, *Adv. Mater.*, 2009, **21**, 2777–2780.
58 L. Z. Zhang, S. X. Du, J. T. Sun, L. Huang, L. Meng, W. Y. Xu, L. D. Pan, Y. Pan, Y. L. Wang, W. A. Hofer and H. J. Gao, *Adv. Mater. Interfaces*, 2014, **1**, 1300104.
59 D. Yi, W. Zhao and F. Ding, *ACS Appl. Nano Mater.*, 2019, **2**, 2921–2925.